CrossMark

Preparation and characterization of biodegradable polyurethanes composites containing thermally treated attapulgite nanorods

Shuenn-Kung Su[1] · Jia-Hao Gu[1] · Hsun-Tsing Lee[2] ·
Cheng-Lung Wu[1] · Chi-Hui Tsou[1] ·
Maw-Cherng Suen[3]

Abstract In this study, polyurethane (PU) was synthesized using 4,4,-diphenyl-methane diisocyanate as a hard segment, polytetramethylene glycol and poly-caprolactone diol as soft segments, and 1,4-butanediol (1,4-BD) as a chain extender. Thermally treated attapulgite (TAT) was added to the PU matrix to prepare TAT/PU nanocomposites. The TEM, FT-IR, XRD and EDS were used to characterize the structure and morphology of the TAT/PU nanocomposites. The TEM results show that TAT maintains its rod-like structure in the PU matrix. The results showed that the addition of a small content of TAT resulted in no obvious changes in the Fourier transform infrared (FT-IR) spectra. XRD results showed that the main crystalline peak of TAT became more pronounced with increasing content of TAT, and EDS showed that the content of Si increased with increasing content of TAT in the TAT/PU nanocomposites. The thermal and mechanical properties were optimal at 2 wt% TAT. When TAT was added at 5 wt%, agglomeration occurred, resulting in a decrease in the thermal and mechanical properties of the TAT/PU nanocomposites. Contact angle and AFM results showed that the hydrophobicity and surface roughness increased with increasing content of TAT. SEM showed that the hydrolytic degradation was affected by the test temperature, test time, and the content of TAT. Moisture absorption tests showed that the moisture absorption of TAT/PU nanocomposites increased with increasing content of TAT and higher environmental humidity.

✉ Maw-Cherng Suen
  sun@tiit.edu.tw

[1] Department of Materials Science and Engineering, National Taiwan University of Science and Technology, Taipei 10607, Taiwan ROC

[2] Department of Materials Science and Engineering, Vanung University, Jongli, Taoyuan 32061, Taiwan ROC

[3] Department of Creative Fashion Design, Taoyuan Innovation Institute of Technology, No. 414, Sec. 3, Jhongshan E. Rd., Jongli, Taoyuan 32091, Taiwan ROC

🌀 Springer

Introduction

Polyurethanes (PUs) are multi-functional materials. Their properties can be tuned and materials of different properties can be synthesized by adjusting the proportions of the synthesis components. Due to this tunability, PUs have been widely investigated for industrial applications, including use in adhesives, medical equipment, paints, and textiles [1–5].

In recent years, many researchers have investigated biodegradable polymers as environmental issues have gradually received increasing attention. Readily biodegradable polyurethanes (PUs) utilize water-degradable polyols, such as polycaprolactone (PCL), polyacrylic acid (PAA), polylactic acid (PLA), and polyglycolic acid (PGA), which possess biological compatibility [6–11]. Some researchers have used PCL as the soft segment of polyurethane, and their results have shown that a higher molecular weight or higher content of PCL is beneficial for the degradation of polyurethanes [12–16].

Organic/inorganic nanocomposites have received considerable attention both in academia and industry. Enhancement materials such as clay, fibreglass, and carbon black have been added to polymer materials [17, 18]. Kim et al. [19] found that montmorillonite can enhance the mechanical properties of waterborne polyur-ethanes. Chen et al. [18] investigated the enhancement effect of sepiolite (Sp) on the thermal properties of PU and showed that the addition of 3 % Sp to PU increased the initial decomposition temperature by 20 °C compared to pure PU. The aforementioned inorganic additives have all been shown to exhibit unique properties and could provide different characteristics to polymers. The use of clays can typically decrease the cost and improve the physical properties of the matrices. However, the intrinsic properties of these clays are often altered after thermal treatment [20–26]. For example, Xu et al. [21] found that after thermal treatment, nanodiamonds exhibited excellent dispersion in various media. Savary et al. [22] found that after thermal treatment, the size of zinc oxide powders was centred at approximately 20 nm. Attapulgite (TAT) is a natural magnesium aluminium phyllosilicate inorganic additive that possesses a unique morphology and rod structure [27] and has been widely used in adsorbents, catalysts, rheological agents, and additives [28–31]. Because attapulgite exhibits a large specific surface area after thermal treatment [32], it can improve the interface compatibility between organic and inorganic materials. Thus, it is expected that the physical properties of polymers will be improved with the addition of attapulgite. So the thermally treated TAT was added to the PCL-based PUs to improve the mechanical properties as tensile strength and hardness of the polymer matrix in this paper.

In summary, The PCL-based PUs and TAT have, respectively, their useful characteristics. However, to the best of our knowledge, no relevant information has been published on the biodegradable PCL soft segment in PU and TAT

nanocomposites. However, it is very important to understand the interfacial interactions of the TAT in the PU chains based on PCL, i.e. the hydrogen bonding interactions among OH groups on TAT surface and NH groups in PU. Therefore, in this present study, attapulgite was first calcined in a high-temperature oven and then added to biodegradable PU synthesized from 4,4′-diphenylmethane diisocyanate (MDI), polycaprolactone diol (PCL) and 1,4-butanediol. The effect of different content of TAT on the structure, morphology, thermal properties, mechanical properties, hydrolytic degradability, and moisture absorption of the PU was investigated.

Experimental

Synthesis of TAT/PU nanocomposites

4,4′-Diphenylmethane diisocyanate (MDI), polycaprolactone diol (PCL, $M_n = 530$) (PCL) and, 1,4-butane diol were purchased from Aldrich. Polytetramethylene glycol (PTMG, $M_w = 1000$) was obtained from Polyscience Co., USA. N,N-Dimethylacetamide (DMAc) was obtained from Mallinckrodt Chemicals. TAT was purchased from Nanjin Yadong Aotu Mining Co., and purified according to the method of Pan et al. [33]. The specific surface area of AT was 95.3 m^2/g.

The attapulgite was thermally treated by heating to 600 °C for 2 h in a high-temperature oven to prepare thermally treated TAT, and the specific surface area was 118.2 m^2/g. In this experiment, polycaprolactone (PCL) and polytetramethylene glycol (PTMG) used as a soft segments, and 4,4,-diphenylmethane diisocyanate (MDI) used as a hard segment were dissolved in DMAc. While mixing with a mechanical mixer at a speed of 200 rpm, the mixture was reacted for 2 h at 75 °C forming a prepolymer. The chain extender 1,4-butanediol (1,4-BD) was then added and reacted for 1 h to form polyurethane (Scheme 1). The TAT/DMAc solution was then dispersed in an ultrasound oscillator and added to the freshly synthesized polyurethane solution in the reactor at 75 °C and stirred by a mechanical mixer. The speed of the mechanical mixer was increased to 500 rpm to blend the mixture for 1 h. TAT/PU nanocomposites were finally obtained. The formulation of the soft and hard segments for PU and the proportion of added TAT are shown in Table 1. The molecular weight distribution of PU relative to polystyrene standards was measured using a gel permeation chromatographer (Jasco model PU-2080 plus) with tetrahydrofuran as a carrier solvent. The weight average molecular weight (M_w) of PU was 45,749 g/mole with a polydispersity index of 1.6.

Specific surface area analysis

The specific surface area of the samples (TAT) was measured using a Micromeritics ASAP2020 instrument (USA). The surface area of TAT was calculated using the Brunauer–Emmett–Teller (BET) equation.
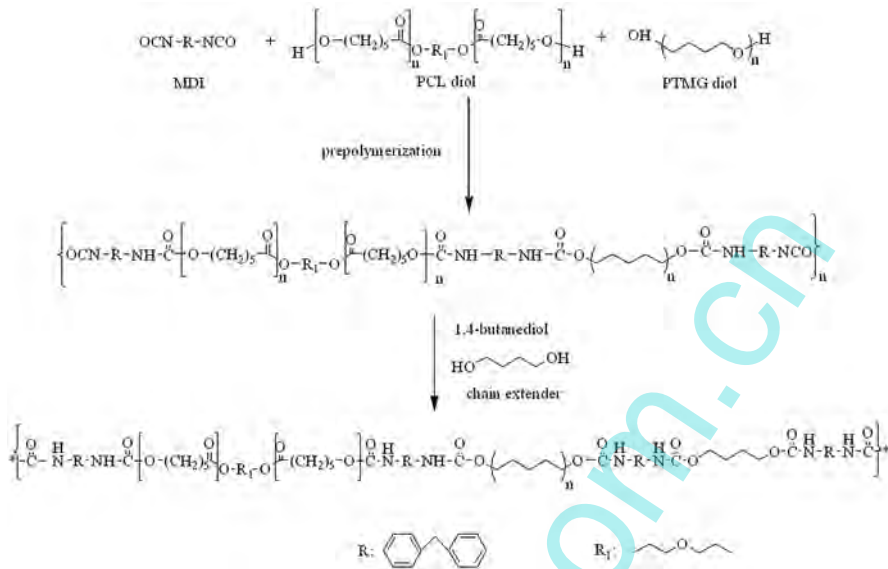
Scheme 1 Synthesis formula for the PU

Table 1 Formulas of the TAT/PU nanocomposites

Designation	MDI (moles)	PTMG (moles)	PCL (moles)	1,4-BD (moles)	TAT (wt%)
PU	4	2.5	1.0	0.5	0
TAT/PU-1	4	2.5	1.0	0.5	0.5
TAT/PU-2	4	2.5	1.0	0.5	1.0
TAT/PU-3	4	2.5	1.0	0.5	2.0
TAT/PU-4	4	2.5	1.0	0.5	5.0

Gel permeation chromatography (GPC)

A gel permeation chromatograph (Analytical Scientific Instruments Model 500) with a reflection index (RI) detector (Schambeck RI2000) and two columns in a series consisting of a Jordi gel DVB mixed bed and a 10,000 Å bed at 30 °C was used to measure the molecular weight distribution relative to polystyrene standards. The calibration curve was obtained using eight standards with molecular weights ranging from 3420 to 2.57×10^6. Tetrahydrofuran was used as the carrier solvent at a flow rate of 1 ml/min.

Transmission electron microscopy analysis

A transmission electron microscope (TEM, Hitachi model H-7500) was used to examine the morphology of the TAT/PU nanocomposites. The samples for TEM examination were first prepared by placing the nanocomposite films into epoxy

capsules and curing the epoxy at 70 °C for 24 h in an oven. The cured epoxies containing TAT/PU nanocomposites were then microtomed with a diamond knife into 70–90-nm-thick slices at −100 °C. Finally, a 3-nm-thick carbon layer was deposited on the slices placed on 200-mesh copper grids for TEM observation.

Fourier transform infrared spectroscopy (FT-IR)

Fourier transform infrared spectroscopy measurements were performed using a PerkinElmer spectrometer (model Spectrum One). Spectra of the samples were obtained by averaging 16 scans with a wavenumber range of 4000–650 cm^{-1} and a resolution of 2 cm^{-1}.

Energy-dispersive X-ray spectroscopy (EDS)

Elemental compositions of the TAT/PU complexes were examined using an energy-dispersive X-ray spectroscopy analyser (Horiba, model 7021-H). Specimens of 2×2 cm^2 were fixed on a sample holder using conductive adhesive tape and were then coated with a thin layer of gold to improve the image resolution. The samples were photographed at 1 K magnification.

X-ray diffraction (XRD)

X-ray diffraction was performed using a Rigaku diffractometer (model RU-H3R). The X-ray beam used Ni-filtered CuKa radiation from a sealed tube operated at 60 kV and 300 mA. Data were obtained in the 2θ range of 5°–70° with a scanning interval of 0.05°.

Thermogravimetric analysis (TGA)

Thermogravimetric analysis was performed using a thermogravimetric analyser (PerkinElmer, model Pyris 1). Samples (5–8 mg) were heated from room temperature to 700 °C under nitrogen at a rate of 10 °C/min.

Differential scanning calorimetry (DSC)

Differential scanning calorimetry was performed on a PerkinElmer DSC, model Jade. Samples were sealed in aluminium pans with a perforated lid. The scans (−80 to 30 °C) were performed with a heating rate of 10 °C/min under nitrogen purging. The glass transition temperatures (T_g) can be located as the midpoints of sharp descent regions in the recorded curves. Samples of approximately 5–8 mg were used for all tests.

Dynamic mechanical analysis (DMA)

Dynamic mechanical analysis was performed using a SEIKO analyser (model SII Muse, DMS6100) at 1 Hz with a 5 μm amplitude over a temperature range of −80

to 30 °C and at a heating rate of 3 °C/min. DMA was conducted using tension mode and specimen dimensions of 20 mm × 5 mm × 0.2 mm (L × W × H). T_g was taken as the peak temperature of the glass transition region in the tan δ curve.

Stress–strain testing

Tensile strength and elongation at break were measured using a universal testing machine (MTS QTEST5, model QC505B1). Testing was conducted according to ASTM D638 specifications. The dimension of the film specimens was 45 mm × 8 mm × 0.2 mm.

Hardness

The hardness of the AT/PU nanocomposite film was measured according to ASTM 2240 specifications using a GS-702 Shore A instrument.

Surface roughness analysis

Atomic force microscopy (AFM) scans were performed using a CSPM5500 instrument from Being Nano-instruments. Generally, there are two types of imaging modes, i.e. tapping and contact modes. Tapping mode was used in this study such that the oscillating probe cantilever causes the tip to make only intermittent contact with the sample. With respect to the phase of the sine wave driving the cantilever, the phase of the tip oscillation is highly sensitive to various sample surface characteristics. Therefore, the tip can also sense the phase images of the sample surface in addition to the topography. The specimens were cut from TAT/PU nanocomposite films with different clay contents.

Contact angle

Contact angles between the samples and deionized water were measured using a Face instrument (model CA-VP150) at room temperature. Dynamic advancing and receding contact angles were recorded while water was added to and withdrawn from the drop, respectively, using a syringe pump. Each reported contact angle is the average value from 3 to 4 drops.

Hydrolytic degradation tests

The hydrolytic degradation of the specimens was evaluated in a 3 % aqueous NaOH solution at 45 °C for various test durations. The specimens were then washed with distilled water and completely dried in a vacuum oven at 70 °C for 3 h. The extent of degradation was determined based on weight loss according to the following equation:

$$\text{Weight loss} = \frac{W_0 - W_t}{W_0} \times 100 \%$$

where W_0 is the dry weight before the degradation test, and W_t is the dry weight at time t. The dimension of the specimens was 2×2 cm^2.

Morphology analysis

The morphology of the specimens at various stages of hydrolytic degradation was observed using a Hitachi scanning electron microscope (SEM), model SU1510. Specimens of 2×2 cm^2 were fixed on a sample holder using conductive adhesive tape and were subsequently coated with a thin layer of gold to improve the image resolution. The samples were photographed at 0.5 K magnification.

Moisture absorption

The thickness of the samples used in the adsorption isotherm test was 0.5 mm. The samples were completely dried at 100 °C for 12 h in an oven. The samples were placed in a standard temperature humidity chamber, and the weight percentage of the samples was measured for the first 120 min. The adsorption time was then gradually increased with a gradual decrease in the adsorption rate [33]. The adsorption and time dependency was finally obtained.

Results and discussion

Structure and morphology

The solution dispersion method was used to mix TAT and PU for the synthesis of TAT/PU nanocomposites in this study. TEM images of TAT in the PU matrix are shown in Fig. 1. For TAT/PU-3 (Fig. 1a), the nano-structure of TAT is observed. Some TAT rods are densely overlapped and randomly oriented, and the morphology resembled rod fibres. The diameter is less than 100 nm, and the length ranges from
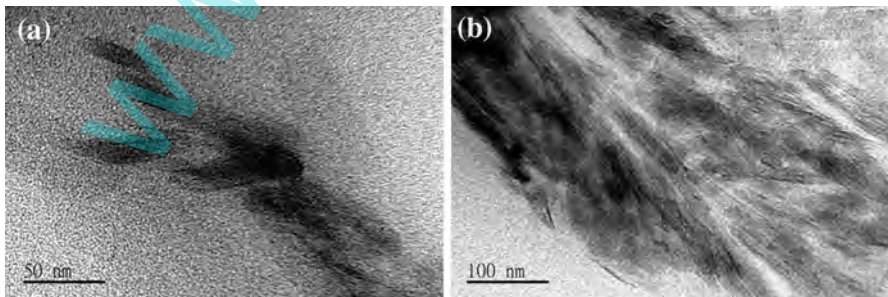

Fig. 1 TEM micrographs of the TAT/PU nanocomposites: **a** TAT/PU-3 and **b** TAT/PU-4

hundreds of nanometres to several micrometres. It is found that TAT exhibits large specific surface area. When the TAT content increases, the degree of TAT agglomeration becomes higher as in Fig. 1b for TAT/PU-4.

The tensile fracture surfaces of TAT/PU shown in Fig. 2 demonstrate that the fracture surface of TAT/PU-01 exhibits a smooth morphology. A slight wrinkle morphology is also observed due to the hard segment. With the addition of a small content of TAT, the fracture surface shown in Fig. 2b changed to present a wrinkled and non-smooth surface. This effect was also observed when the content of TAT was further increased, as shown in Fig. 2c, d. A small content of irregular TAT was dispersed within the PU matrix, indicating that there was a strong interaction
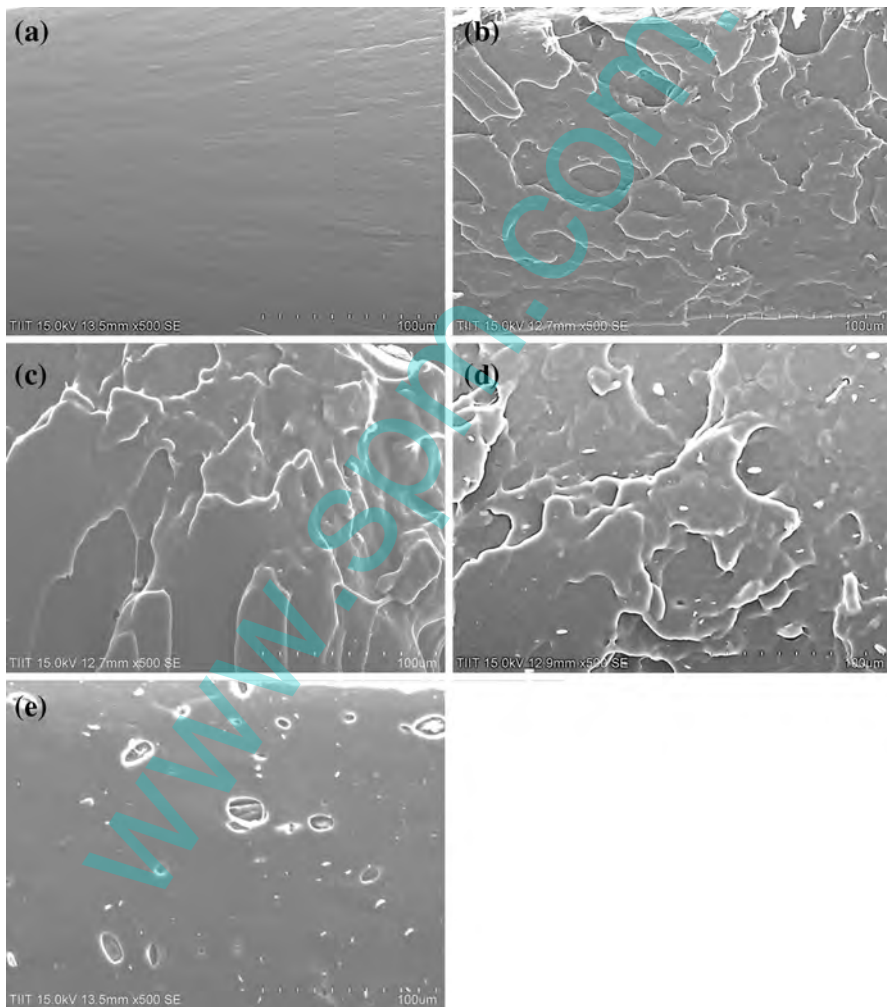

Fig. 2 SEM photographs of fractured section of the TAT/PUs nanocomposites: **a** PU, **b** TAT/PU-1, **c** TAT/PU-2, **d** TAT/PU-3 and **e** TAT/PU-4

between the PU matrix and the TAT enhancement material and that the adhesion of TAT in the PU matrix was very good. However, with a further increase in the content of TAT, the wrinkled and non-smooth surface changed to a smooth surface, and agglomeration occurred as shown in Fig. 2e. The size of the TAT fibres increased and the distribution was uneven, likely because excellent dispersion and interfacial adhesion could not be realized with an excessive content of TAT in the PU matrix. It can be expected that the thermal and mechanical properties will decrease due to this phenomenon.

The FT-IR spectra of the TAT/PU nanocomposites are shown in Fig. 3. The five polymers showed similar functional groups. There is stretching vibration peak of the N–H group at 3316 cm^{-1}. There is no absorption band at 2400–2300 cm^{-1} in each spectrum that is the stretching vibration absorption band of –NCO groups, indicating that MDI was completely consumed. The peaks at 2940 and 2855 cm^{-1}, 1729 and 1706 cm^{-1}, 1597, 1220, and 1106 cm^{-1} are attributed to CH$_2$ stretching vibration, C=O, C=C stretching vibration, C–O stretching vibration, and ether group C–O–C stretching vibration, respectively. However, due to the small content of TAT in the PU matrix, none of the characteristic functional groups of TAT were present in the spectra.

Figure 4 shows the EDS images of the TAT/PU nanocomposites. The contents of silicon measured in TAT/PU-1, TAT/PU-2, TAT/PU-3, and TAT/PU-4 were 2.66, 5.91, 8.13, and 11.8 %, respectively. The EDS images show that the Si content increased with increasing TAT content. In addition, EDS images indicate that the Si distribution became denser with increasing TAT content and obvious agglomeration occurred in TAT/PU-4.

The XRD spectra of the TAT/PU nanocomposites are shown in Fig. 5, and they show that the characteristic crystallization peaks of TAT occur at $2\theta = 8.3°$, $13.6°$, $20°$, and $26.6°$, respectively. The results are in agreement with the diffraction peaks
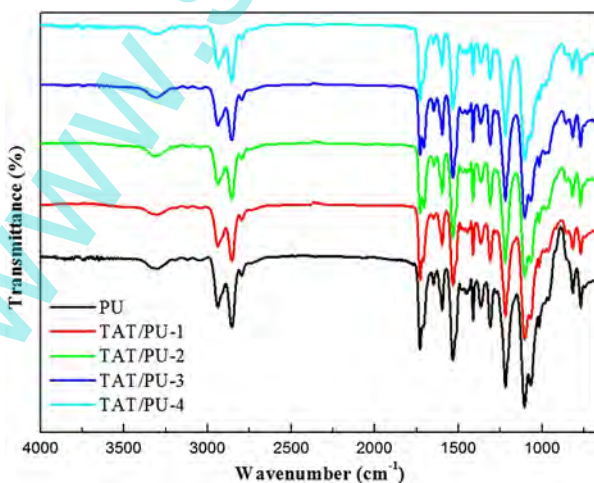

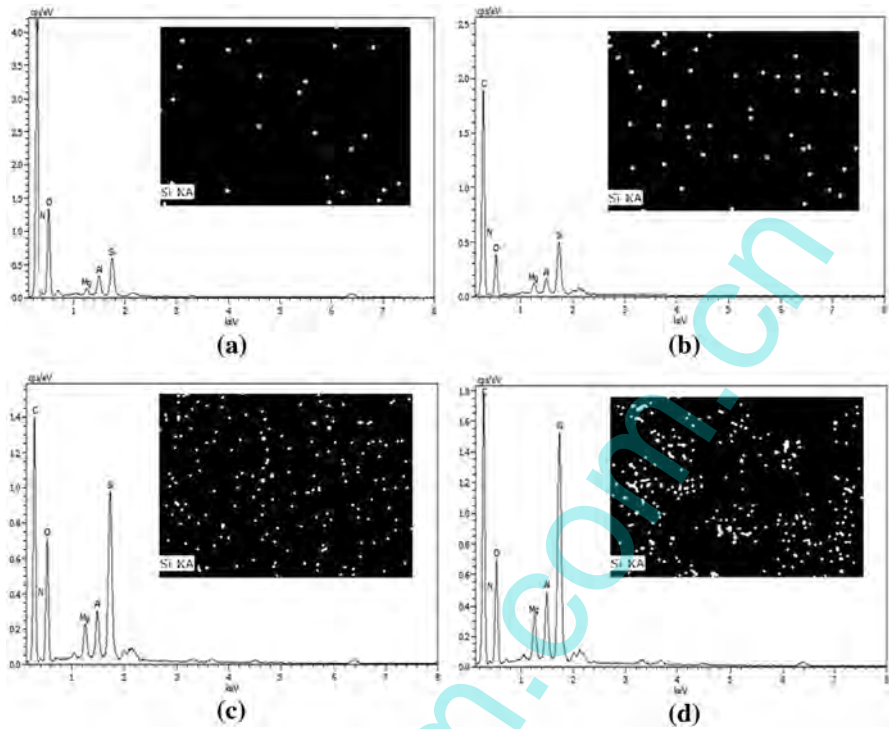**Fig. 3** FT-IR spectra of the TAT/PUs nanocomposites

Fig. 4 EDS images of the TAT/PU nanocomposites: **a** TAT/PU-1, **b** TAT/PU-2, **c** TAT/PU-3, **d** TAT/PU-4
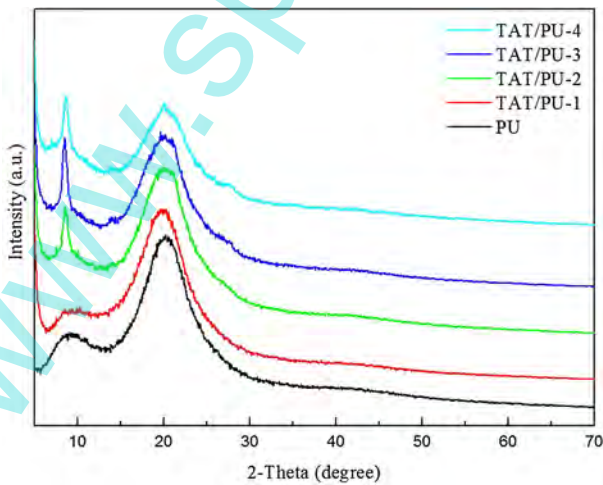

Fig. 5 XRD patterns of the TAT/PU nanocomposites

observed by Wang et al. [27]. The XRD diffraction pattern of PU that contains no TAT shows two broad peaks at around 8.3° and 20°. Since sharp peaks are associated with crystalline morphology, the above two broad peaks indicate the morphology is not crystalline. These two broad peaks are associated with the local morphology of PU that is somewhat orderly but is not crystalline. For the TAT/PU-2, -3, and -4, a sharp peak at 8.3° is observed. In addition, the peak height at 8.3° relative to that at 20° is higher with increasing TAT content. This sharp peak at 8.3° is associated with the crystalline morphology of agglomerated TAT, and the peak intensity increases with increasing TAT content. But for the TAT/PU-1, no sharp peak at 8.3° is observed, so the TAT in TAT/PU-1 is well dispersed and is not aggregated. In other words, the presence of crystallization peak at around 8.3° means agglomeration of TAT, and the peak intensity or crystallization degree increases with increasing TAT content, i.e. the agglomeration degree of TAT increases with increasing TAT content. If TAT is well dispersed, there is no crystallization peak at around 8.3°.

Thermal properties

The TGA curve for the TAT/PU nanocomposites is shown in Fig. 6a, and the DTG curve is shown in Fig. 6b. Each of the differential curves shows two decomposition peaks. The lower temperature is attributed to the decomposition of urethane group, which is designated as T_{max1}, and the decomposition at high temperature is related to the polyol, which is designated as T_{max2}. The two decomposition temperatures for all TAT/PU nanocomposites are listed in Table 2. With an increased content of TAT in TAT/PU nanocomposites, T_{max1} and T_{max2} increased. The T_{max1} for PU and TAT/PU-3 was 336.5 and 348.7 °C, respectively. In addition, the T_{max2} was 412.4 and 425.3 °C, respectively. These results suggest that the addition of TAT resulted in an improvement in the thermal resistance of PU.

However, the T_{max1} and T_{max2} of TAT/PU-4 are lower than those of TAT/PU-2 and TAT/PU-3. This phenomenon may be explained by the amount of TAT agglomerates present in the nanocomposite. When TAT content is very high as in TAT/PU-4 (5 wt% TAT), many TAT agglomerates were formed and some overlapped and became channels for the heat conduction as shown in Fig. 1b. Attapulgite (TAT) is one kind of natural clay [34]. Its thermal conductivity (0.68 W/(mK), [35]) is substantially higher than that (0.177 W/(mK), [36]) of PU. The heat from the surrounding heater is much easier to be conducted into the bulk of nanocomposite through the connected TAT agglomerates than through the PU phase. The bulk of composite was subject to a higher thermal attack when the outer heat is easier to be conducted into the interior part through higher amount of TAT agglomerates. Then the composite had a lower thermal degradation temperature. The amount of connected TAT agglomerates of TAT/PU-4 is higher than that of TAT/PU-2 (1 wt% TAT) or TAT/PU-3 (2 wt% TAT), so the heat from the surrounding heater is easier to be conducted into the bulk of TAT/PU-4. Therefore, the degradation temperature of TAT/PU-4 is lower than that of TAT/PU-2 or TAT/PU-3. Excess inorganic additives caused a lower degradation temperature of a nanocomposite was also reported in some literatures [37]. But the cause was not
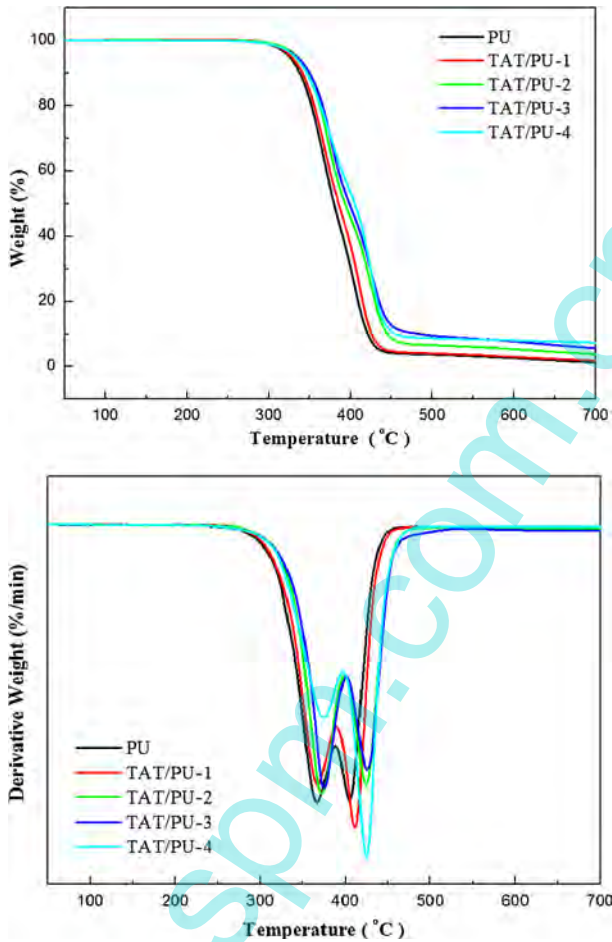
Fig. 6 TGA curves of the TAT/PU nanocomposites

Table 2 Thermal properties of the TAT/PU nanocomposites

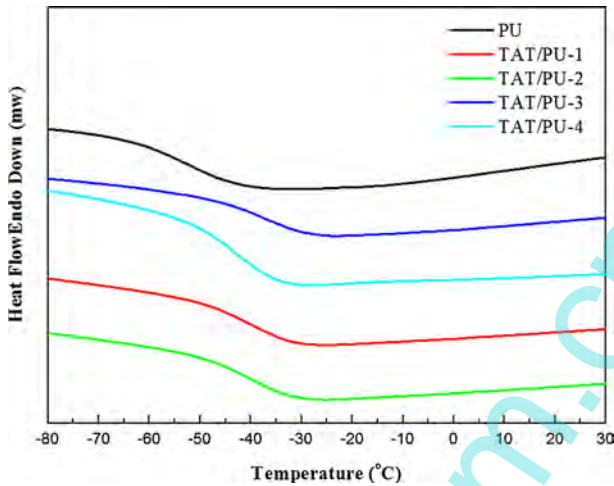| Designation	TGA			DSC	DMA
	T_{max1} (°C)	T_{max2} (°C)	Residue at 700 °C (%)	T_g (°C)	T_{gd} from tan δ (°C)
PU	336.5	412.4	1.3	−58.8	−33.8
TAT/PU-1	338.6	412.6	1.8	−44.8	−25.6
TAT/PU-2	344.5	417.5	3.8	−42.0	−23.4
TAT/PU-3	348.7	425.3	5.6	−40.8	−15.8
TAT/PU-4	341.4	415.0	7.3	−45.7	−32.6

Fig. 7 DSC thermograms of the TAT/PU nanocomposites

explained therein. The different thermal conductivities between TAT agglomerates and PU moiety may be a possible explanation. In addition, when heated to 700 °C, the residual weights of PU, TAT/PU-1, TAT/PU-2, TAT/PU-3, and TAT/PU-4 are 1.3, 1.8, 3.8, 5.6 and 7.3 %, respectively. The residual weight increases with increasing content of TAT, indicating that TAT is not combustible.

Figure 7 shows the DSC curve for the TAT/PU nanocomposites. The T_g for the TAT/PU nanocomposites were −58.8, −44.87, −42.03, −40.78, and −45.78 °C, which are listed in Table 2. These results indicate that the T_g for the TAT/PU nanocomposites increased with increasing content of TAT. This effect occurred because rigid structure of TAT hinders the segmental motion of PU. No crystalline peaks typical of endothermic and exothermic processes were observed in the DSC curves, thereby confirming the presence of TAT and indicating that PU remained in an amorphous state, which is in agreement with the XRD results.

The tan δ curve for the TAT/PU nanocomposites is shown in Fig. 8. Typically, the highest point in the tan δ curve is defined as the dynamic glass transition temperature (T_{gd}). The T_{gd} for the PU, TAT/PU-1, TAT/PU-2, TAT/PU-3, and TAT/PU-4 were −33.8, −25.6, −23.4, −15.8, and −32.6 °C respectively, which are listed in Table 2. These results suggest that with an increased content of TAT, the T_{gd} of the TAT/PU nanocomposites increased. However, an excess content of TAT caused agglomeration, resulting in a decrease in T_{gd} for PU. This finding was in good agreement with the DSC results.

Mechanical properties

Figure 9 shows the stress–strain curve for the TAT/PU nanocomposites, and the results are listed in Table 3. The maximum stress values for PU, TAT/PU-1, TAT/PU-2, TAT/PU-3, and TAT/PU-4 were 5.3, 8.2, 9.1, 11.2, and 6.1 MPa,
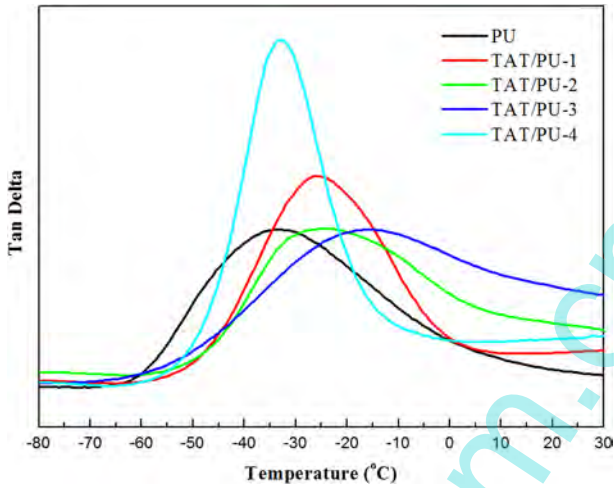
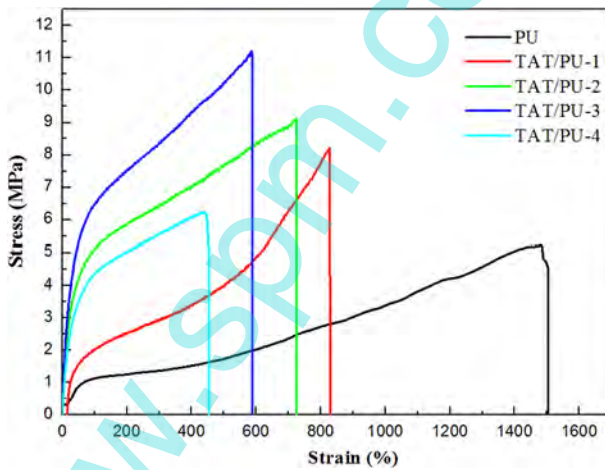**Fig. 8** Tan δ curves of the TAT/PU nanocomposites

Fig. 9 Tensile properties of the TAT/PU nanocomposites

Table 3 Tensile properties of the TAT/PU nanocomposites

Sample	Maximum stress (MPa)	Strain at break (%)	Hardness (°)
PU	5.3	1495.0	82
TAT/PU-1	8.2	828.2	85
TAT/PU-2	9.1	724.4	86
TAT/PU-3	11.2	585.7	88
TAT/PU-4	6.1	444.9	89

respectively. These results indicate that the maximum stress increased with increasing content of TAT, which can be attributed to two factors. First, after the thermal treatment, the increase in the specific surface area of TAT improved the interfacial interaction between PU and TAT. Second, the large aspect ratio of TAT improved its interaction with the PU matrix. However, when the content of TAT was increased to 5 wt%, the maximum stress deceased, likely because the excess content of TAT caused agglomeration in the PU matrix, resulting in brittleness and a decrease in the mechanical properties of the samples. The elongation at break of PU, TAT/PU-1, TAT/PU-2, TAT/PU-3, and TAT/PU-4 were 1192.1, 28.2, 724.4, 585.7, and 444.9 %, respectively. Among the PU materials, PCL has excellent ductility. However, the addition of rigid TAT caused PU materials to transform from soft and ductile to hard and brittle.

The results shown in Table 3 indicate that the minimum and maximum hardness values of the TAT/PU nanocomposites were 82° and 89°, respectively. The test results show that with an increased content of TAT, the hardness of the TAT/PU nanocomposites increased. This increase occurs because TAT is a rigid enhancement material, and its addition can improve the hardness of the PU matrix.

Surface properties

The 3D morphologies and phases for the TAT/PU nanocomposites are shown in Fig. 10. Similar 3D morphologies and phases were observed. Certain disturbances are present in both figures. The PU without the addition of TAT displayed its original surface and morphology, whereas there were apparent changes after the addition of TAT. Compared to the images of PU without TAT, dramatic changes occurred after the addition of TAT. Particularly, when TAT was added at 5 wt%, many large granules were present, and the phase image showed an abundance of isolated small domains having irregular granular or channel-like morphologies. The continuous, dark areas correspond to PU in the phase image. The brighter areas are enriched with TAT. The phase images for TAT/PU-4 indicate that most of the TAT was aggregated on the surface of the PU matrix. Table 4 lists the roughness averages of the TAT/PU nanocomposites, and the average roughness values for the TAT/PU nanocomposites were 2.2, 3.66, 4.47, 5.73, and 8.82 nm when the content of TAT was increased from 0 to 5 wt%. These results indicate that TAT caused an increase in the surface roughness of the TAT/PU nanocomposites.

Figure 11 shows the contact angles for the TAT/PU nanocomposites. The contact angles for PU, TAT/PU-1, TAT/PU-2, TAT/PU-3, and TAT/PU-4 are 82.2°, 86.9°, 88.5°, 90.6°, and 92.2°, respectively. These results indicate that the contact angle for the TAT/PU nanocomposites increased with increasing content of TAT. This finding can be attributed to the nano-scale surface roughness of TAT/PUs. The surface roughness is of nano-scale as shown in Table 4 of the AFM results. The TAT/PU with more TAT possesses more nano-scale protrusions as lotus leaves that can prevent the adsorption of water. So the TAT/PU with more TAT possesses higher contact angle.

Fig. 10 AFM topographic and phase images of the TAT/PU nanocomposites with different TAT contents. TAT content: **a** 0 wt%; **b** 0.5 wt%; **c** 1.0 wt%; **d** 2.0 wt%; **e** 5.0 wt%. 3D morphology: **a1**, **b1**, **c1**, **d1**, **e1**. Phase: **a2**, **b2**, **c2**, **d2**, **e2**
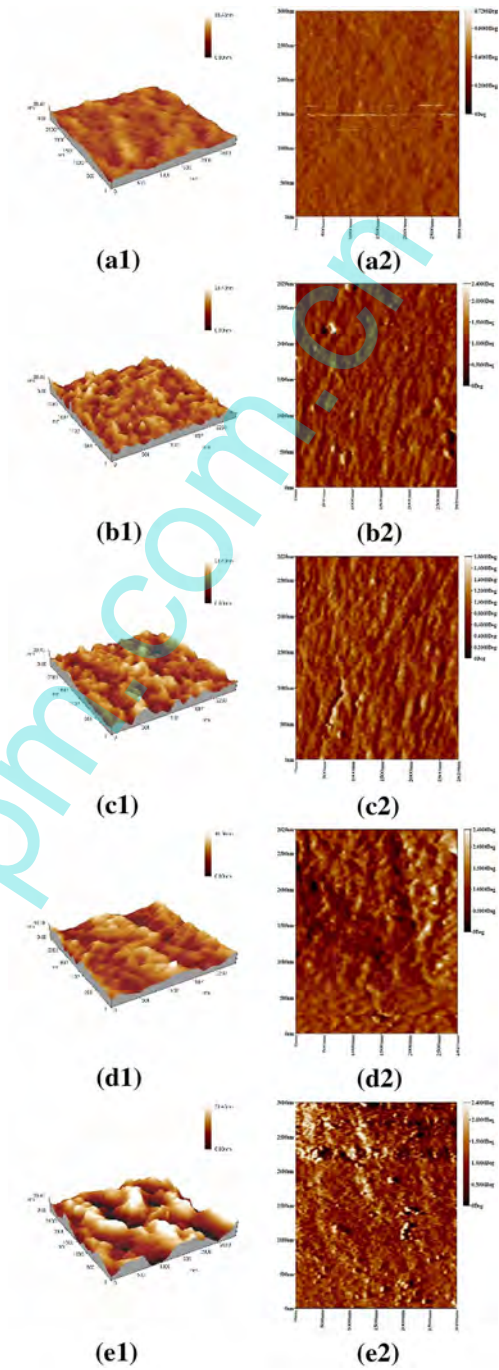

(a1) (a2)

(b1) (b2)

(c1) (c2)

(d1) (d2)

(e1) (e2)

Table 4 Surface roughness data of the TAT/PU nanocomposites

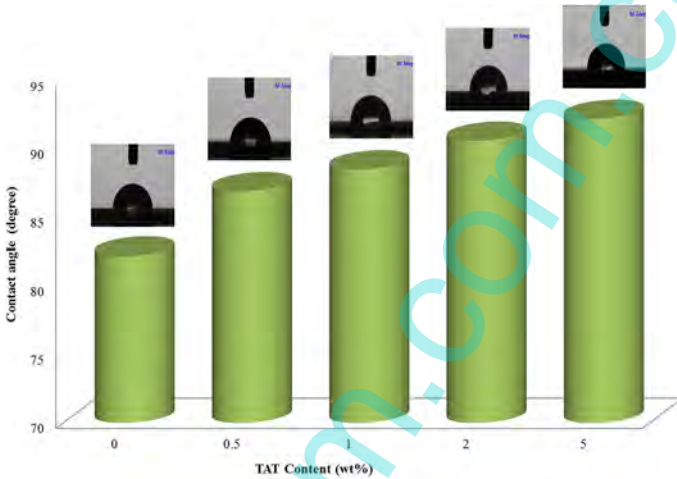| Sample	Ra (nm)
PU	2.20
TAT/PU-1	3.66
TAT/PU-2	4.47
TAT/PU-3	5.73
TAT/PU-4	8.20

Fig. 11 Surface properties of the TAT/PU nanocomposites

Hydrolytic degradation and morphology analysis

Figure 12a, b shows the results of hydrolytic degradation test of the TAT/PU nanocomposites at 37 and 45 °C, respectively. The weights of all samples decreased with increasing test time, test temperature and TAT content. The samples were
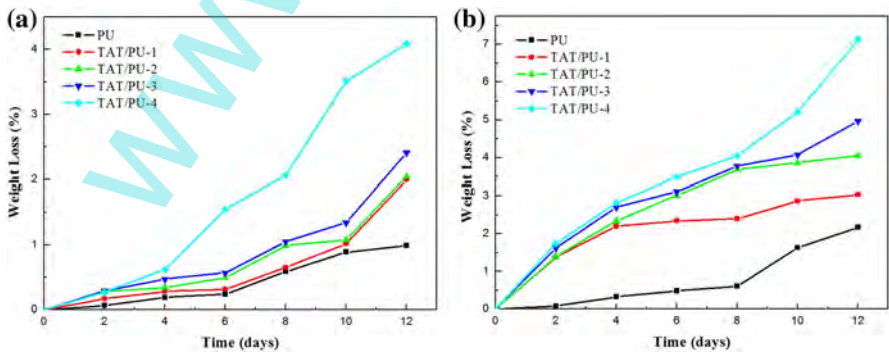

Fig. 12 Hydrolytic degradation results of the TAT/PU nanocomposites at 37 °C (**a**) and 45 °C (**b**)

etched with a 3 % aqueous NaOH solution. There are two possible factors that influence the hydrolytic degradation tests. The first one is the phase structure. Hydrolytic degradation usually occurred at the aliphatic chains in a random fashion, and the rate of degradation was largely determined by the crystallinity of the polymer, the crystallite size and the structure. Because water molecules can easily diffuse into the amorphous regions of the polymer, the hydrolytic degradation of the polymer will preferentially start in the amorphous region rather than in the crystalline regions. Figure 12a, b shows that an increasing content of TAT raises the rate of hydrolytic degradation of PU. Tang et al. [35] synthesized polycarbonate urethanes and investigated their cholesterol esterase catalysed hydrolysis. Their results showed that the degree of hydrolytic degradation of the polymer was largely dependent on the interaction of the hard segments on the surfaces of the polymers. Similar results were obtained by Jeong et al. [17]. In their study, the addition of montmorillonite to PU led to decreased phase separation and weaker interactions between hard segments. The observed hydrolytic degradation of TAT/PU nanocomposites was similar to the aforementioned phenomena. Therefore, water molecules can more easily diffuse into the areas with less phase separation, causing faster degradation of the TAT/PU nanocomposite.

The second factor is the presence of nano-pores in the nanocomposites with TAT agglomerates. When the TAT content is higher than 1 wt% (with TAT/PU-2), there are some TAT agglomerates in the TAT/PU nanocomposites as stated in the discussion of XRD spectrum of TAT/PUs. Agglomerates of TAT have irregular outer surfaces that can result in many small irregular nano-pores among TAT agglomerates and PUs as shown in the SEM photograph of TAT/PU-4 nanocomposite (Fig. 13). In addition, attapulgite itself has many tunnel-like rectangular nano-pores [34]. During the hydrolytic degradation tests, these nano-pores can suck water into the bulk of nanocomposites by the driving pressure of surrounding water
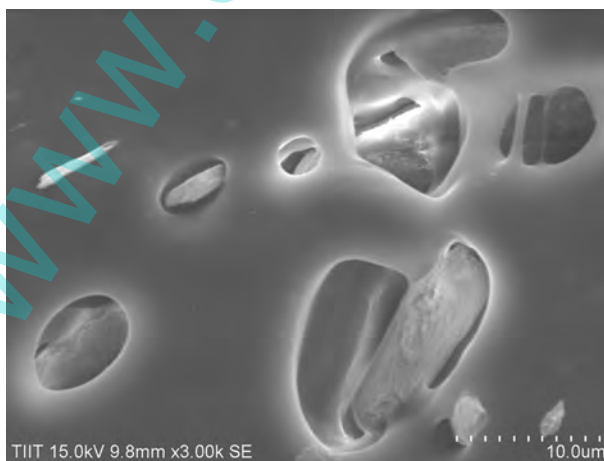

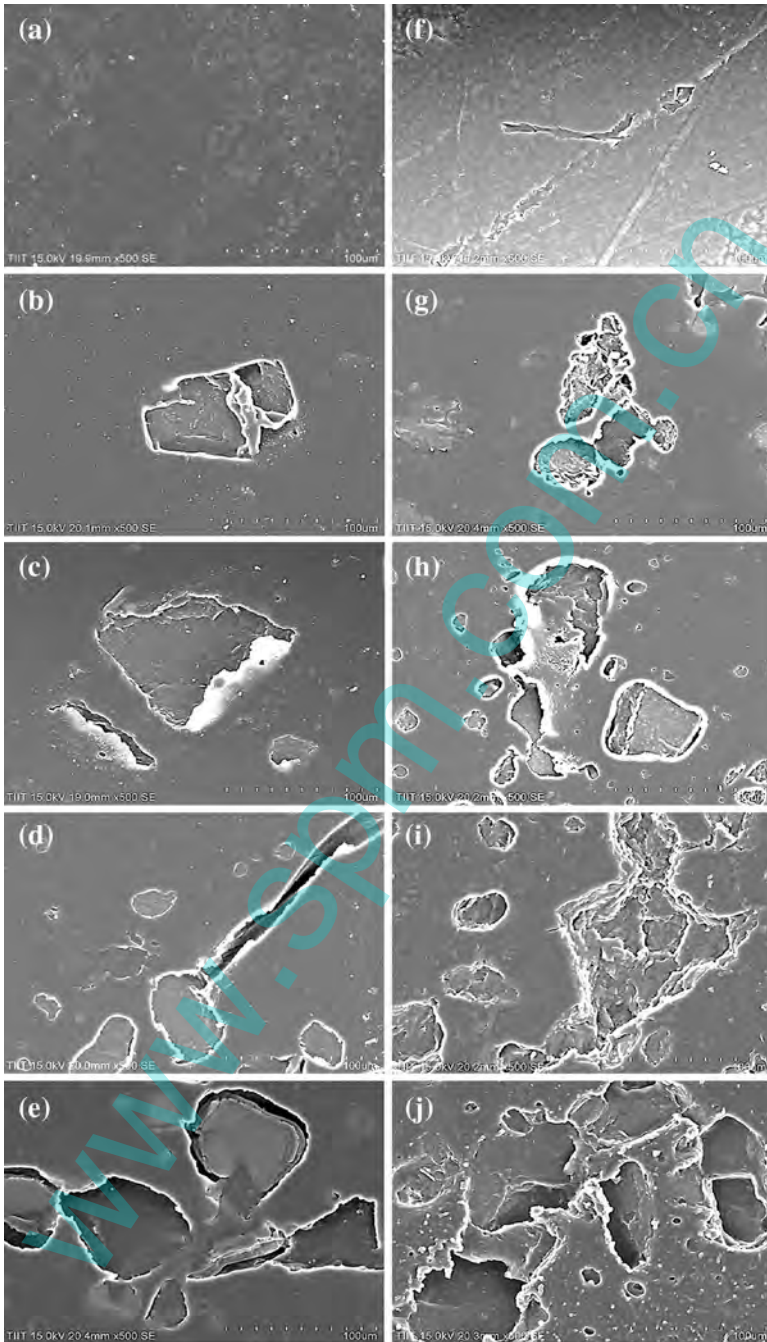**Fig. 13** SEM micrograph of the TAT/PU-4

Fig. 14 SEM micrographs of the **a** PU, **b** TAT/PU-1, **c** TAT/PU-2, **d** TAT/PU-3 and **e** TAT/PU-4 with hydrolytic degradation for 12 days at 37 °C; **f** PU, **g** TAT/PU-1, **h** TAT/PU-2, **i** TAT/PU-3 and **j** TAT/PU-4 with hydrolytic degradation for 12 days at 45 °C

and enhance the hydrolytic degradation. Thus, the degree of hydrolytic degradation of TAT/PUs increases with increasing TAT content.

In addition, the rate of degradation was faster at 45 °C than at 37 °C for all samples. For example, the weight loss was 4.09 % when TAT/PU-4 was held at 37 °C for 12 days, whereas the weight loss was 7.13 % when TAT/PU-4 was held at 45 °C 12 days. This difference occurred because at high temperatures, volume expansion of all sample allows alkaline water molecules to easily enter the structure. Additionally, water molecules move more easily at high temperatures [36].

Scanning electron microscope images of TAT/PU degraded at 37 and 45 °C for 12 days are shown in Fig. 14. The SEM image of PU degraded at 37 °C without the addition of TAT, as shown in Fig. 14a, indicates that wrinkles appeared on the surface of PU. Figure 14b–e shows that with increasing content of TAT, the wrinkles on the surface of PU became deeper and holes appeared. Figure 14f shows an SEM image of PU degraded at 45 °C without the addition of TAT. This image indicates that cracks appeared on the surface of PU. Figure 14g–j shows that with increasing content of TAT, the surface of PU became more fractured, the number of dislocated areas increased markedly, and the depth of holes increased accordingly. These results are in agreement with the above conclusion that volume expansion increased the ability of alkaline water molecules to etch the surfaces.
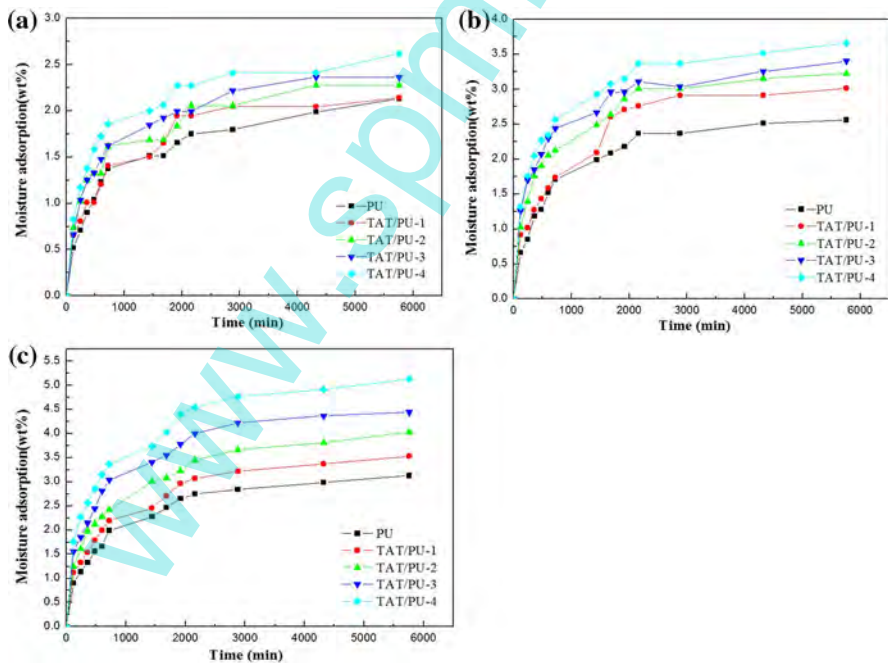

Fig. 15 Dependence of moisture absorption on time: **a** at RH = 70 %; **b** at RH = 80 %; **c** at RH = 90 % by fixing $T = 37$ °C

Moisture absorption rate analysis

Figure 15a–c shows the moisture absorption curves for the TAT/PU nanocomposites at different RH conditions but at a fixing temperature of 37 °C. These results indicate that the rate of moisture absorption for the TAT/PU nanocomposites at RH of 70, 80, and 90 % rapidly increased at 800 min, gradually slowed at 1000 min and reached saturation at 2000 min. However, with increasing RH and content of TAT, the weight increased for all samples. The moisture absorption rate was markedly higher for TAT/PU-4 at RH = 90 %. Factors that influence the moisture absorption tests resemble those of the hydrolytic degradation tests. The first one is the phase structure that water molecules can more easily diffuse into the areas with less phase separation caused by more TAT content. Water molecules first enter the amorphous regions of PU and form hydrogen bonds with -OH groups on the surface of TAT after expansion and wetting. The second one is the presence of nano-pores among TAT agglomerates and PUs on the film surface that facilitates the surrounding moisture to absorb. Therefore, the rate of moisture absorption of TAT/PUs increases with increasing TAT content.

Conclusions

TAT/PU nanocomposites were successfully prepared in this study using the solution dispersion method. The structural and morphological results indicate that TAT had a rod structure and was well dispersed in the PU matrix. The –NCO groups were not observed in the FT-IR spectra, indicating that MDI was completely consumed. XRD analysis showed that with increasing content of TAT in the TAT/PU nanocomposites, the characteristic crystalline peaks for TAT became more pronounced. A broad diffraction peak at $2\theta = 20°$ was observed for the TAT/PU nanocomposites. This peak is a characteristic of PU and showed no evident changes with increasing content of TAT. The EDS analysis showed that the content of Si increased with increasing content of TAT, and EDS mapping indicated that Si showed agglomeration in the TAT/PU nanocomposites having high content of TAT. Thermal analysis showed that the decomposition temperature increased with increasing content of TAT in the TAT/PU nanocomposites. However, when TAT was added at 5 wt%, the thermal stability of TAT/PU decreased. T_g and T_{gd} were increased with increasing content of TAT but decreased when TAT was added at 5 wt%. Analysis of the mechanical properties showed that with increasing content of TAT in TAT/PU, the tensile strength increased and the elongation at break decreased, However, when TAT was added at 5 wt%, the tensile strength and elongation at break of the TAT/PU nanocomposite decreased. The decreases in the thermal and mechanical properties of TAT/PU-4 were due to the agglomeration of TAT. Hardness analysis showed that the hardness of TAT/PU increased with increasing content of TAT. The surface properties of TAT/PU showed that the surface roughness and hydrophobicity increased with increasing content of TAT. The hydrolytic degradation test showed that the rate of degradation increased with increasing temperature, test time, and content of TAT. After hydrolytic degradation, the extent of cracking and displacement of the surface increased with

increasing content of TAT. The moisture absorption test showed that the moisture absorption rate of the TAT/PU nanocomposites increased with increasing TAT content and the environmental humidity.

References

1. Park HB, Lee YM (2002) Separation of toluene/nitrogen through segmented polyurethane and polyurethane urea membranes with different soft segments. J Membr Sci 197:283–296
2. Abraham GA, de Queiroz AAA, San Roman JS (2001) Hydrophilic hybrid IPNs of segmented polyurethanes and copolymers of vinylpyrrolidone for applications in medicine. Biomaterials 22:1971–1985
3. Gugliuzza A, Clarizia G, Golemme G, Drioli E (2002) New breathable and waterproof coatings for textiles: effect of an aliphatic polyurethane on the formation of PEEK-WC porous membranes. Eur Polym J 38:235–242
4. Tien YI, Wei KH (2001) Hydrogen bonding and mechanical properties in segmented montmorillonite/polyurethane nanocomposites of different hard segment ratios. Polymer 42:3213–3221
5. Mequanint K, Sanderson R (2003) Nano-structure phosphorus-containing polyurethane dispersions: synthesis and crosslinking with melamine formaldehyde resin. Polymer 44:2631–2639
6. Huang SJ (1985) Biodegradable polymers. Encyclo Polym Sci Eng 2:220–243
7. Chandra R, Rustgi R (1998) Biodegradable polymers. Prog Polym Sci 23:1273–1335
8. Okada M (2002) Chemical syntheses of biodegradable polymers. Prog Polym Sci 27:87–133
9. Nair LS, Laurencin CT (2007) Biodegradable polymers as biomaterials. Prog Polym Sci 32:762–798
10. Pena J, Corrales T, Izquierdo-Barba I, Doadrio AL, Vallet-Regi M (2006) Long term degradation of poly(ε-caprolactone) films in biologically related fluids. Polym Degrad Stabil 91:1424–1432
11. Coulembier O, Degee P, Hedrick JL, Dubois P (2006) From controlled ring-opening polymerization to biodegradable aliphatic polyester: especially poly(betamalic acid) derivatives. Prog Polym Sci 31:723–747
12. Jiang X, Li JH, Ding MM, Tan H, Ling QY, Zhong YP (2007) Synthesis and degradation of nontoxic biodegradable waterborne polyurethanes elastomer with poly(ε-caprolactone) and poly(ethylene glycol) as soft segment. Eur Polym J 43:1838–1846
13. Ayres E, Oréfice RL, Yoshida MI (2007) Phase morphology of hydrolysable polyurethanes derived from aqueous dispersions. Eur Polym J 43:3510–3521
14. Li FG, Hou JN, Zhu W, Zhang XA, Xu M, Luo XL (1996) Crystallinity and morphology of segmented polyurethanes with different soft-segment length. J Appl Polym Sci 62:631–638
15. Tatai L, Moore TG, Adhikari R, Malherbe F, Jayasekara R, Griffiths I (2007) Thermoplastic biodegradable polyurethanes: the effect of chain extender structure on properties and in vitro degradation. Biomaterials 28:5407–5417
16. Heijkants RGJC, Schwab LW, van Calck RV, de Groot JH, Pennings AJ, Schouten AJ (2005) Extruder synthesis of a new class of polyurethanes: polyacylurethanes based on poly(ε-caprolactone) oligomers. Polymer 46:8981–8989
17. Jeong EH, Yang J, Lee HS, Seo SW, Baik DH, Kim J, Youk JH (2008) Effective preparation and characterization of montmorillonite/poly(ε-caprolactone)-based polyurethane nanocomposites. J Appl Polym Sci 107:803–809
18. Chen H, Lu H, Zhou Y, Zheng M, Ke C, Zeng D (2012) Study on thermal properties of polyurethane nanocomposites based on organosepiolite. Polym Degrad Stabil 97:242–247
19. Kim BK, Seo JW, Jeong HM (2003) Morphology and properties of waterborne polyurethane/clay nanocomposites. Eur Polym J 39:85–91
20. Wang MR, Jia DC, He PG, Zhou Y (2010) Influence of calcination temperature of kaolin on the structure and properties of final geopolymer. Mater Lett 64:2551–2554
21. Xu X, Yu Z, Zhu Y, Wang B (2005) Influence of surface modification adopting thermal treatments on dispersion of detonation nanodiamond. J Solid State Chem 178:688–693
22. Savary E, Marinel S, Colder H, Harnois C, Lefevre FX, Retoux R (2011) Microwave sintering of nano-sized ZnO synthesized by a liquid route. Powder Technol 208:521–525

23. Suciu C, Hoffmann AC, Vik A, Goga F (2008) Effect of calcination conditions and precursor proportions on the properties of YSZ nanoparticles obtained by modified sol-gel route. Chem Eng J 138:608–615

24. Pérez-Barrado E, Pujol MC, Aguiló M, Llorca J, Cesteros Y, Díaz F, Pallarès J, Marsal LF, Salagre P (2015) Influence of acid-base properties of calcined MgAl and CaAl layered double hydroxides on the catalytic glycerol etherification to short-chain polyglycerols. Chem Eng J 264:547–556

25. Essaidi N, Samet B, Baklouti S, Rossignol S (2014) Feasibility of producing geopolymers from two different Tunisian clays before and after calcination at various temperatures. Appl Clay Sci 88–89:221–227

26. Zeng L, Cao DY, Xu Y, Fan CW, Peng XQ (2014) Novel method for preparation of calcined kaolin intercalation compound-based geopolymer. Appl Clay Sci 101:637–642

27. Wang Z, Zhou Y, Sun Y, Fan K, Guo X, Jiang X (2009) Helical polyurethane@attapulgite nanocomposite: preparation, characterization and study of optical activity. J Solid State Chem 182:2130–2134

28. Wang CH, Shieh YT, Guo G, Nutt S (2010) Effects of organophilic-modified attapulgite nanorods on thermal and mechanical behavior of segmented polyurethane elastomers. Polym Composite 31:1890–1898

29. Lu H, Shen H, Song Z, Shing KS, Tao W, Nutt S (2005) Rod-like silicate-epoxy nanocomposites. Macromol Rapid Commun 26:1445–1450

30. Wang CH, Auad ML, Marcovich NE, Nutt S (2008) Synthesis and characterization of organically modified attapulgite/polyurethane nanocomposites. J Appl Polym Sci 109:2562–2570

31. Chen F, Lou D, Yang J, Zhong M (2011) Mechanical and thermal properties of attapulgite clay reinforced polymethylmethacrylate nanocomposites. Polym Advan Technol 22:1912–1918

32. Boudrichea L, Calvetc R, Hamdi B, Balard H (2012) Surface properties evolution of attapulgite by IGC analysis as a function of thermal treatment. Colloid Surf A 399:1–10

33. Vogt BD, Soles CL, Lee HJ, Lin EK, Wu W (2005) Moisture absorption into ultrathin hydrophilic polymer films on different substrate surfaces. Polymer 46:1635–1642

34. Xiang L, Pan YC, Zeng GF, Jiang JL, Chen J (2016) Preparation of poly(ether-block-amide)/attapulgite mixed matrix membranes for CO_2/N_2 separation. J Membr Sci 500:66–75

35. Akinyemi OD, Sauer TJ, Onifade YS (2011) Revisiting the block method for evaluating thermal conductivities of clay and granite. Int Commun Heat Mass 38:1014–1018

36. Zhao JC, Du FP, Cui W, Zhu P, Zhou XP, Xie XL (2014) Effect of silica coating thickness on the thermal conductivity of polyurethane/SiO_2 coated multiwalled carbon nanotube composites. Compos Part A Appl S 58:1–6

37. Zhang Y, Shen J, Li Q, Pang L, Zhang QY, Xu ZS, Yeung KWK (2013) Synthesis and characterization of novel hyperbranched polyimides/attapulgite nanocomposites. Compos Part A Appl S 55:161–168